Automated ablation stakes to constrain temperature-index melt models

Andrew David Wickert[1,2,3] (iD), Katherine Ruth Barnhart[4,*] (iD),

William Henry Armstrong[5] (iD), Matías Romero[6,7] (iD), Bobby Schulz[1,8,9] (iD),

Gene-Hua Crystal Ng[1,2] (iD), Chad Timothy Sandell[1,3], Jeff La Frenierre[10] (iD),

Shanti Bhattacharya Penprase[1,2,†] (iD), Maximillian Van Wyk de Vries[1,2,‡] (iD) and

Kelly Revenaugh MacGregor[11] (iD)

[1]Department of Earth & Environmental Sciences, University of Minnesota, Minneapolis, MN 55455, USA; [2]Saint Anthony Falls Laboratory, University of Minnesota, Minneapolis, MN 55414, USA; [3]Northern Widget LLC, Saint Paul, MN 55105, USA; [4]Department of Geological Sciences and Institute for Arctic and Alpine Research, University of Colorado Boulder, Boulder, CO 80309, USA; [5]Department of Geological and Environmental Sciences, Appalachian State University, Boone, NC 28608, USA; [6]Centro de Investigaciones en Ciencias de la Tierra (CICTERRA) – Consejo Nacional de Investigaciones Científicas y Técnicas (CONICET), Universidad Nacional de Córdoba, CP: X5016GCA Córdoba, Provincia de Córdoba, Argentina; [7]Department of Geoscience, University of Wisconsin, Madison, WI 53706, USA; [8]Department of Electrical & Computer Engineering, University of Minnesota, Minneapolis, MN 55455, USA; [9]GEMS Agroinformatics Initiative, University of Minnesota, St. Paul, MN 55108, USA; [10]Department of Environment, Geography and Earth Sciences, Gustavus Adolphus College, St. Peter, MN 56082, USA and [11]Department of Geology, Macalester College, St. Paul, MN 55105, USA

*Present address: U.S. Geological Survey, Geologic Hazards Science Center, Golden, CO 80401, USA.

†Present address: Department of Earth Sciences, Dartmouth College, Hanover, NH 03755, USA.

‡Present address: Department of Geography, University of Cambridge, Cambridge CB2 3EL, UK, and Department of Earth Sciences, University of Cambridge, Cambridge CB3 0EZ, UK.

Abstract

We developed automated ablation stakes to measure colocated *in situ* changes in relative glacier-surface elevation and climatological drivers of ablation. The designs, refined over 10 years of development and deployments, implement open-source hardware and common building materials. The ablation stakes record distance to the snow/ice surface, air temperature and relative humidity every 1–15 min. Using these high-frequency data, we demonstrate that melt factors calculated using standard melt-rate vs temperature regressions converge over averaging windows of approximately 12 h or greater. Furthermore, we evaluate an integral approach to estimating temperature-index melt factors for ablation. In a test case on Glaciar Perito Moreno, Argentina, this integral approach reveals an overall positive-degree-day melt factor of 7.5 mm w.e. $°C^{-1}$ d^{-1}. We describe four deployments with iteratively improved designs and provide a list of materials required to construct an automated ablation stake.

1. Introduction

Future projections of glacier mass balance require accurate predictions of how climate and its changes affect ice ablation. This in turn affects the future trajectory of glaciers, which play critical roles in freshwater supply (e.g. Meier, 1969; Andermann and others, 2012; Somers and others, 2019; Saberi and others, 2019), sea-level change (e.g. Meier and others, 2007; Jacob and others, 2012; Hay and others, 2012; Larour and others, 2017) and landscape stability and associated natural hazards (e.g. Temme, 2015; Deline and others, 2021; Veh and others, 2022; Van Wyk de Vries and others, 2022; Wetterauer and others, 2022). Substantial efforts have been undertaken to both model (e.g. Hock, 2003; Hock and Holmgren, 2005) and measure (e.g. Popovnin and others, 1999; Karpilo Jr, 2009; Zemp and others, 2009; Immerzeel and others, 2014; La Frenierre and Mark, 2014) glacial ice ablation. Combinations of models and measurements are required to advance our capacity to extrapolate current glacier mass balance and predict future ice loss (Machguth and others, 2006).

Approaches to modeling ablation range from temperature-index methods (Ohmura, 2001; Hock, 2003), in which air-temperature and ablation-rate data (typically from field-monitoring campaigns) are compared via a linear regression, to full energy-balance calculations (Hock and Holmgren, 2005). So-called 'enhanced temperature-index' approaches fall between these two end-members, and typically incorporate solar radiation alongside temperature (Hock, 1999; Pellicciotti and others, 2005; Carenzo and others, 2009) into a multi-parameter empirical approach. Critically, all three of these methods require field data on climatic drivers as well as on ice-surface lowering, with the latter for calibration and/or validation (e.g. Walter and others, 2005).

Ablation measurements have long been made using traditional *ablation stakes*, rods placed into holes drilled in the ice and re-surveyed by hand (e.g. Stuefer and others, 2007; Braithwaite, 2008; Brook and Paine, 2012; Minowa and others, 2023). While these measurements provide critical *in situ* data, they are limited in temporal resolution, which may in turn limit both their utility and spatial extent. Manually measured ablation stakes provide data at single points that must be revisited every time a measurement is to be made, with typical repeat times of days to months. Additionally, local climatic drivers of ablation between these measurements are not recorded, thereby requiring extrapolation to weather stations. Such extrapolations require

assumed lapse rates (Wheler and others, 2014), which can differ substantially between on-ice and terrestrially grounded temperature-measurement stations (Anderson and others, 2014, DR.1). Furthermore, the labor required to repeatedly measure these non-automated stakes places logistical limits both on the number of ablation stakes that may be installed and on the extent of the ablation-stake network. This is compounded by weather-dependent safety concerns regarding glacier travel, which may in turn systematically bias when and under which conditions repeat measurements are made. Additionally, local temperature is sensitive to surface composition, be it ice, snow or debris (e.g. Hagg and others, 2008), and the associated surface albedo. Paired, automated measurements of temperature (and other climatic drivers) may improve ablation-model predictions.

To date, scientists have explored a number of approaches toward measuring ablation at high temporal resolution. Hulth (2010) used a tensioned draw wire to measure net ice-surface ablation while mechanically avoiding the impacts of fresh snow-fall. Gabbud and others (2015) performed repeat glacier surveys using a terrestrial laser scanner (TLS) over hourly time scales, and Voordendag and others (2021) characterized and tested a permanent TLS installation on the Hintereisferner Gletscher (Austria). Netto and Arigony-Neto (2019) designed a data-logging station to slide down a 12 m self-collapsing ablation stake, using radio-frequency identification (RFID) tags to detect each 15 cm of melt. Landmann and others (2021) measured ablation via automated repeat photos of ablation stakes.

Our work here follows a long history of development and deployment of ultrasonic rangefinders to measure glacier ablation (or accumulation). Labine and Koerner (2004) developed a network of ultrasonic rangefinders and temperature sensors across the Canadian arctic in the late 1980s. Oerlemans (2000) deployed a Campbell Scientific ultrasonic rangefinder on a fixed post atop the Morteratschgletscher in Switzerland – alongside a weather station that slid downwards as the ice surface ablated – to monitor accumulation and ablation at a site. Oerlemans and others (2004) and Munro and others (2004) deployed networks of on-glacier automated weather stations. Braun and others (2004) deployed an on-glacier temperature and ultrasonic-ranging station at the Vernagtferner ice mass. The Icelandic Glacier Automatic Weather Stations (ICE-GAWS) network (cf. Gunnarsson and others, 2021) includes ultrasonic rangefinders for snow depth and ice-surface ablation. Gusain and others (2009) likewise used an ultrasonic sensor in their study combining energy and mass balance in East Antarctica. Keeler and Brugger (2012) later tested a pair of inexpensive ultrasonic rangefinders on Storglaciären in Sweden, again to measure the distance to the snow and/or ice surface. They demonstrated that even consumer- or hobbyist-grade instruments could be useful for glaciological research. Wickert (2014) and Wickert and others (2019) provided data from ultrasonic rangefinders (of a different model than those used by Keeler and Brugger, 2012), thermistors, and (Wickert and others, 2019, only) inclinometers that measure glacier-surface-elevation change and air temperature. Sold and others (2021) applied computer-vision techniques to track melt around traditional ablation stakes. Fausto and others (2021) present the PROMICE network of weather stations, including ablation stakes, with coverage across Greenland. These stations include ultrasonic rangefinder readings alongside station-tilt measurements and pressure-transducer readings of ablation.

Here we move from the prototype stage demonstrated in our earlier work toward a reproducible automated ablation stake to capture high temporal resolution data on both the amount of ablation and its drivers. The instrumentation to automate these ablation stakes adds little weight (∼1.5 kg), costs ∼US$700 (in year 2022) and can be assembled in the field within 15–30 min. Having co-located and high-resolution climatic driver data
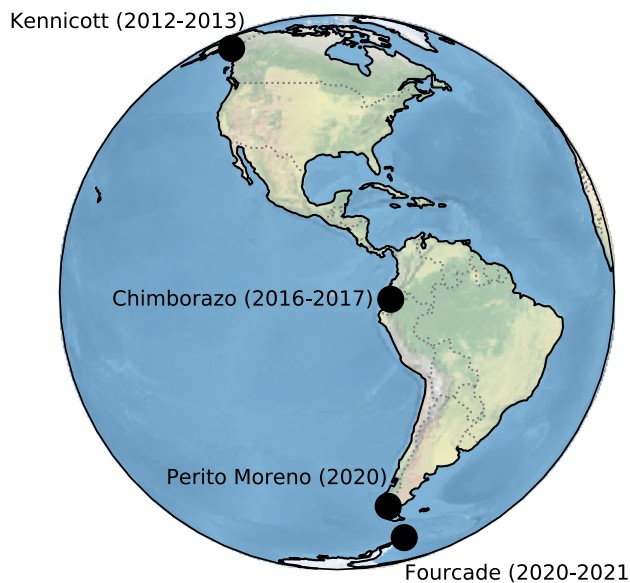

Figure 1. Field-deployment sites and their associated years of active data collection. Data for these deployments as well as those in Minnesota, USA (seasonal snowpack) and Glaciar Hermoso, Cayambe, Ecuador are available via GitHub and archived through Zenodo (Wickert and others, 2023).

alongside equally high-resolution information on ice-surface elevation should improve melt-factor calculation (cf. Hock, 2003) and enable observations of changing melt factors over time. Furthermore, their assistance in generating measurements that are dense in space (rapid deployment; reduced need to visit sites) can help to characterize differing melt rates as a function, for example, of ice properties, debris, elevation and temperature.

Our automated ablation stake design is open source, as is its firmware stack (Schulz and Wickert, 2020, 2022a, 2021a; Schulz, 2021; Schulz and Wickert, 2022c) and much of its electronic hardware (Wickert, 2019; Schulz, 2021; Schulz and Wickert, 2022b). Furthermore, Wickert (2023) provides a guide toward assembling and deploying an automated ablation stake. This combination of freely available resources is critical to reducing the cost and improving the reproducibility of the automated ablation stake and its data, especially through studies led by and run through academic and/or non-profit institutions. As such, its open-source and limited-cost design contributes directly to meeting scientific objectives.

We illustrate automated ablation-stake deployments and development efforts from 2012 to 2021 (data: Wickert and others, 2023). These include field research on Kennicott Glacier (Alaska, USA: Wickert, 2014; Armstrong and Anderson, 2020), Glaciares Reschreiter and Hans Meyer (Chimborazo, Ecuador: Tauro and others, 2018; Saberi and others, 2019; Wickert and others, 2019), Glaciar Hermoso (Cayambe, Ecuador), Glaciar Perito Moreno (Santa Cruz, Argentina) and Glaciar Fourcade (Kopuła Warszawy, King George Island, Antarctica), as well as on seasonal snowpack (Saint Paul, Minnesota, USA) (Wickert, 2014; Tauro and others, 2018; Saberi and others, 2019; Wickert and others, 2019; Armstrong and Anderson, 2020; Wickert and others, 2023). Here we highlight four of these glacier deployments (Figs 1, 2) and describe the design behind the ablation stakes that enabled these measurements. Our goal is for these stakes to expand the reach of monitoring networks and improve databases for ablation modeling.

2. Design

The automated ablation-stake design consists of four elements: (1) a device to measure ablation as a function of time, (2) one or more sensors to measure ambient weather conditions that may
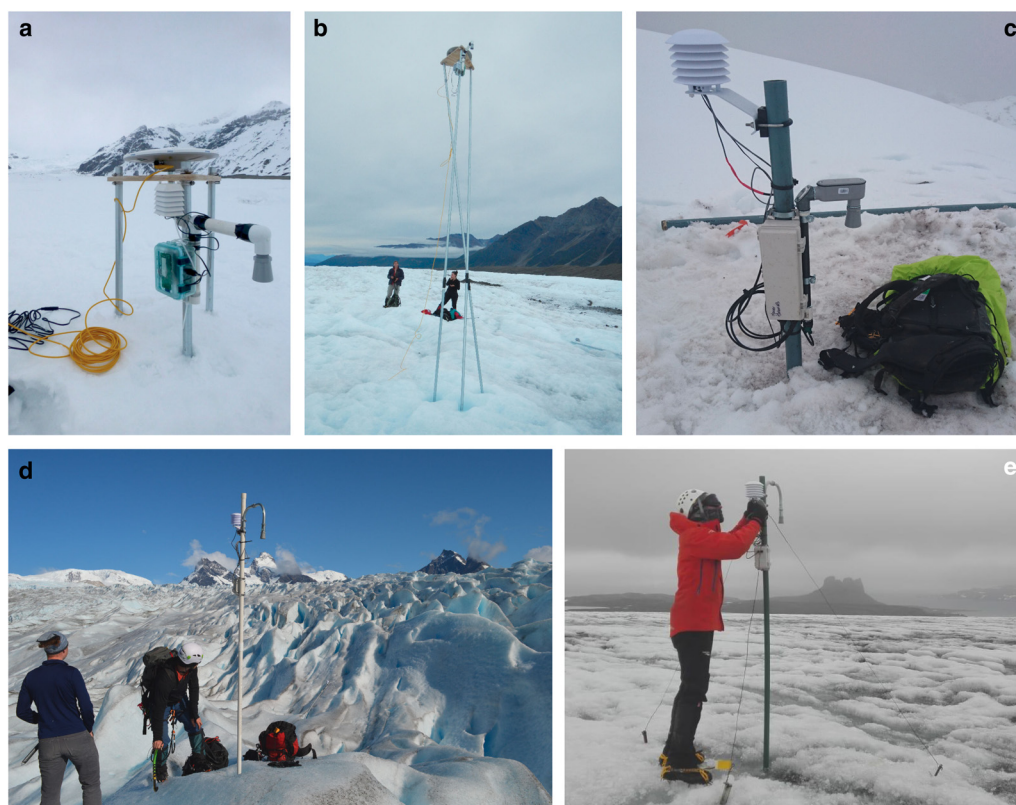
Figure 2. Automated ablation-stake deployments. (a, b) Kennicott Glacier, Alaska, USA: (a) Installation, 17 May 2012; (b) after melt season, 16 September 2013 (possibly a different station). Pictured: (left) Billy Armstrong and (right) Katy Barnhart. (c) Glaciar Hans Meyer, Chimborazo, Ecuador: 29 June 2016. (d) Glaciar Perito Moreno, Argentina: 13 March 2020. Pictured: (left) Max Van Wyk de Vries and (right) Andy Wickert. (e) Glaciar Fourcade, King George Island, Antarctica: 25 January, 2021. Pictured: Matias Romero.

drive ice-melt rates, (3) a data logger to operate these sensors and record the information that is returned, and (4) a physical structure to hold the sensors and data logger and serve as a stable mounting point for distance measurements. Based on four separate deployments (Fig. 2), we developed a set of recommendations for designing and constructing automated ablation stakes (Table 1). Here we describe our decisions and rationale toward each of the four required elements.

Table 1. Recommended design elements for future automated-ablation-stake designs and installations alongside those used for our four deployments

	Recommended	Kennicott (2012–2013)	Chimborazo (2016–2017)	Perito Moreno (2020)	Fourcade (2020–2021)
Anchoring in glacier	Multiple points of contact (reduce tilt, rotation)	3× 3/4-inch EMS conduit	1× 5-cm HDPE pipe	1× 5-cm PVC pipe	1× 5-cm PVC pipe + 3× staked guy wires
Weather measurements	Temperature and relative humidity (Amphenol Telaire T9602)	T (CanTherm CWF1B103F3380, Vishay-Dale PTF5610K000BYEB)	T (CanTherm CWF1B103F3380, Vishay-Dale PTF5610K000BYEB); T, RH (HM1500LF)	T, RH (Amphenol Telaire T9602)	T, RH (Amphenol Telaire T9602)
Data logger	Margay[a]	ALog BottleLogger[b]	ALog BottleLogger[b]	Margay[a]	Margay[a]
Rangefinder	Maxbotix MB7388[c]	Maxbotix MB7060[d]	Maxbotix MB7389[e]	Maxbotix MB7386[c]	Maxbotix MB7386[c]
Rangefinder wiring	MaxBotix Helper[f]	Directly soldered	Directly soldered	MaxBotix-Helper[c]	MaxBotix-Helper[c]
Rangefinder cable	Alpha Wire 5004C	Unknown 4-wire cable	Belkin 4-wire cable	Alpha Wire 5004C	Alpha Wire 5004C
Rangefinder mount	EMS conduit U	PVC with threaded elbow	3/4" threaded LB-type conduit body	EMS conduit U	EMS conduit U
Mount–mast attachment	2 × hose clamps	2 × hose clamps	2 × conduit hangers, bolted through pipe	2 × hose clamps	2 × hose clamps
Inclinometer	STMicroelectronics LIS3DHTR	–	Murata SCA100T-D02-1	–	–
Batteries	3× AA	3× D	3× D	3× AA	3× AA
Enclosure	WH-04 Polycarbonate with clear lid	GSI small box	Polycase WH-08	Polycase WH-04	Polycase WH-04
Solar radiation shield	Dwyer Series RHRS 6-plate	Onset RS1	Dwyer Series RHRS 6-plate	Dwyer Series RHRS 6-plate	Dwyer Series RHRS 6-plate

T, temperature; RH, humidity.
[a] Schulz and Wickert (2022b).
[b] Wickert (2014); Wickert and others (2019).
[c] 1 mm resolution; 500–9999 mm range.
[d] 1 cm resolution; 20–765 cm range.
[e] 1 mm resolution; 300–5000 mm range.
[f] Wickert (2019).

2.1 Measuring ablation: ultrasonic rangefinder

We recommend measuring ablation by determining the distance from a fixed point above the ground to the snow and/or ice surface using a MaxBotix brand ultrasonic rangefinder (cf. Evans, 2016; Tauro and others, 2018; Wickert and others, 2019), model MB7388 (500–9999 mm range), which is IP67-rated for waterproofness. These rangefinders measure the two-way travel time of an emitted 'ping' of sound and report the distance to the surface creating the largest acoustic return. They are sensitive to targets spanning a ~0.3 m radius centered on the rangefinder. Although the MB7388 is not a model that we used in any of our past deployments (Table 1), it combines two features we found most helpful from sensors that we did use, namely the longer range of the MB7386 with the strongest-target filtering of the MB7389. The MB7388 returns data via a TTL serial protocol: Data are sent as a series of bits, in which a high voltage is interpreted as '1' and a low voltage is interpreted as '0', at a baud rate of 9600 bps. This data rate is slow enough that its outputs can be reliably interpreted by software emulations of a serial port as well as by true hardware serial receivers, thereby permitting it to be connected to a wider range of data-logging microcontrollers. The MB7388 is precise to 1 mm and accurate to < 1%; if desired, multiple range measurements may be made to obtain more complete distance statistics.

We chose these ultrasonic rangefinders instead of laser rangefinders (e.g. LiDAR Lite v3 HP) for two reasons. First, the 6-order-of-magnitude slower speed of sound than light in air permits higher precision distance measurements even with substantially less precise timekeeping. In this case, the LiDAR Lite is precise to 10 mm and accurate to ±25 mm (targets ≥2 m distant) or ±50 mm (targets <2 m distant) based on tests with water surfaces (Paul and others, 2020). Second, the ultrasonic rangefinder returns the distance to the largest acoustic reflector within the path of its ~30 cm-radius beam. Therefore, it can filter out local-scale roughness – for example, snow bedforms (Kochanski and others, 2019) and variability in ice melt – better than the mm-scale point measurements from a laser rangefinder or manual measurements to the base of an ablation stake.

We connect a temperature-correction unit ('HR-MaxTemp') to the ultrasonic rangefinder to correct for the temperature-dependent speed of sound in air. We house this inside a Dwyer Series RHRS 6-plate solar radiation shield. This corrects for an approximately $0.19\%\ ^\circ C^{-1}$ error in the distance measurement, which corresponds (for example) to ± 4 mm $^\circ C^{-1}$ when the rangefinder is ~2.1 m from the ice surface.

We wire the MaxBotix ultrasonic rangefinder to both the data logger and its MaxTemp temperature-correction circuit through the open-source MaxBotix-Helper circuit board (Fig. 3; design and assembly information available from Wickert, 2019), which provides screw-terminal connections to MaxBotix ultrasonic rangefinders. It addresses three issues that we experienced during development, assembly and installation. First, the MaxBotix-Helper attaches to the ultrasonic rangefinder with a stiff seven-pin header (Fig. 3c) that spans all of its solder rings, providing a stable connection platform despite the small amount of metal around each ring on the rangefinder for soldering. Second, connecting the cable to a screw terminal allows the cable to be replaced if it breaks, and therefore, for functional sensors to be reused following cable failure. Finally, multiple connections need to be made to the ground (GND) solder ring on the rangefinder; such connections are more difficult to make and may be more easily broken. Therefore, the MaxBotix-Helper provides three screw-terminal connections to individual ground pins to ensure that one is available per required connection (Fig. 3b). In addition to solving these three issues, the solder jumper on the MaxBotix-Helper
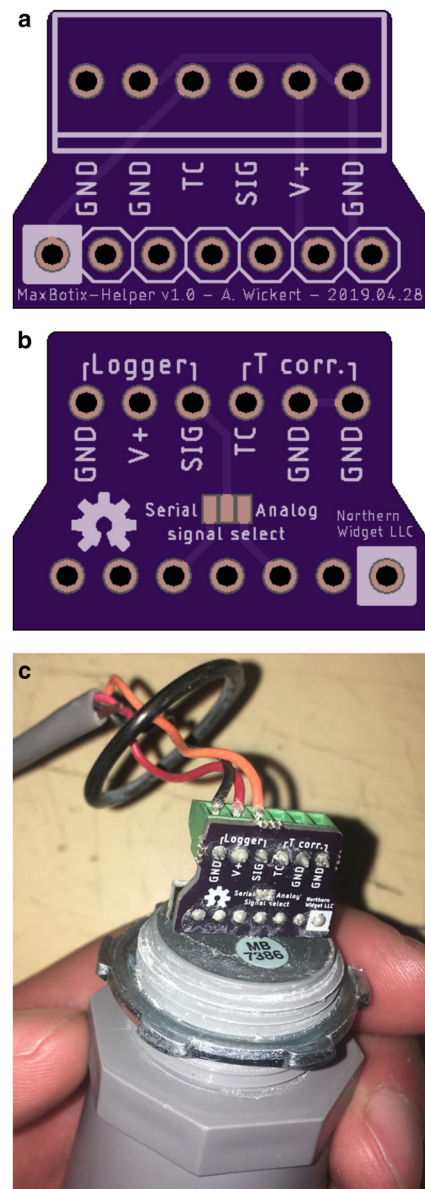

Figure 3. MaxBotix-Helper. (a) Circuit-board front. Platform for soldering the 0.1-inch (2.54 mm) pitch screw-terminal header block denoted. Screw-terminal pins labeled as follows: GND: ground; TC: temperature compensation; SIG: signal, which could be either an analog voltage or a digital serial signal; V+: positive voltage (2.7–5.5 V). White square corresponds to the square on the MaxBotix silkscreen, which denotes pin 1. Image generated by OSH Park. (b) Circuit-board back. Screw-terminal pins are grouped into those intended for the logger and those intended for the MaxTemp temperature correction. The solder jumper is used to select whether the SIG pin outputs a serial signal or an analog voltage. Image: OSH Park. (c) MaxBotix-Helper installed and connected to a Margay data logger (Schulz and Wickert, 2022b). Photo: Matias Romero, Base Carlini, King George Island, Antarctica.

permits the user to select an analog voltage or serial output to appear on the SIG pin. The analog voltage derives from the the serial output, and is provided in case a data logger has no available serial-receive pin.

An optional but helpful part of any ablation-measurement system is an inclinometer to measure the angle between the distance-measurement device (e.g. ultrasonic rangefinder) and the vertical. This can show if the automated ablation stake has been disturbed, correct inclined measurements to vertical distance, and indicate when to no longer trust the vertical distance data (Wickert and others, 2019, Fig. 5; data from Chimborazo, Ecuador). We used a Murata SCA100T-D02-1 (Table 1), which is no longer in

production. Based on our use of the STMicroelectronics LIS3DHTR MEMS accelerometer as an inclinometer in a separate design (Schulz, 2019), we recommend incorporating it in future designs (Table 1).

In order to record the distance to the ice surface over time, the ultrasonic rangefinder must be connected to a data logger. Open-source (e.g. Arduino-compatible) data loggers provide an effective and low-cost option (e.g. Wickert, 2014; Beddows and Mallon, 2018). We initially wrote custom code for each data-logger deployment (cf. Wickert and others, 2019), and have now produced an open-source library that provides a standardized API and pre-built functions to communicate with the MaxBotix ultrasonic rangefinder via software-serial methods ('MaxBotix_Library': Schulz and Wickert, 2020).

Our primary goal in measuring distance is to calculate ablation rate. However, the ultrasonic rangefinders will also measure accumulation. In the example below, no accumulation occurs, thereby simplifying data processing.

2.2 Climatic drivers: temperature and relative humidity

Major drivers of glacier energy balance include incoming short-wave radiation, outgoing longwave radiation, and air temperature (e.g. Litt and others, 2019). Wind speed and humidity measurements can also be made to help constrain sublimation (e.g. MacDonell and others, 2013). At lower elevations and higher atmospheric pressures, temperature alone can serve as a suitable proxy for energy balance (Litt and others, 2019).

We measure climatic drivers of ablation on the same stakes used to record ice-surface lowering. This avoids problems of inter-polation or extrapolation of climatic data to the ablation-stake sites. Three considerations with this approach are that: (1) the measurements occur over an ice surface, (2) the measurement elevation above the ice surface may change with time, and (3) the stakes will eventually melt out and fall over. We consider these below.

Our earliest ablation stakes measured temperature alone using a thermistor and reference resistor (Table 1, Kennicott and Chimborazo). We connected these via a voltage divider to the 10-bit analog–digital converter (1024 total measurement increments) on the ALog data logger (Wickert, 2014; Wickert and others, 2019; Armstrong and Anderson, 2020). This provided ~0.1°C resolution temperature data (Table 1; Figs 2a,b).

Our more recent designs incorporate the IP67-rated Amphenol Telaire T9602 relative-humidity and temperature sensor, for which Schulz and Wickert (2022c) wrote an open-source Arduino-compatible library that implements a standardized API. The T9602 returns data at 14-bit precision (16 384 total measurement increments) with accuracies of ±2% relative humidity and ±0.5°C. Its IP-rated waterproof status is important: the potential for rapid melt atop a glacier can create a cold and humid environment that promotes condensation and could ruin unprotected sensors. The T9602 is our preferred sensor because it has proven robust in multiple field deployments, adds only modest additional cost and no additional design complexity (cf. Schulz, 2021) over a more basic temperature sensor, adds an additional measurement usable for an energy balance, and includes a round cable that enables a tight seal via the cable-gland gasket to keep moisture out of the data-logger box.

2.3 Data logger: Margay

Our designs implement the open-source and Arduino-compatible data loggers that we have developed since 2011 (Wickert, 2014; Wickert and others, 2019; Schulz, 2021; Schulz and Wickert, 2022b). We suggest such a data logger for the following three reasons: (1) Open-source systems are commonly inexpensive (Beddows and Mallon, 2018; Ensign and others, 2019; Wickert and others, 2019), and instruments mounted on ablation stakes atop glaciers may be lost. (2) Arduino-compatible designs can take advantage of the sensor libraries that we have developed (Schulz and Wickert, 2020, 2022c). (3) Arduino-compatible open-source devices have built-in interfaces to communicate with the MaxBotix ultrasonic rangefinder (hardware or software serial), the T9602 temperature and relative-humidity sensor (I^2C bus) and thermistors on voltage dividers (analog–digital converter).

Our preferred data logger is the Margay, developed since late 2017 by Schulz and Wickert (2021b, 2022b). It is small (42.3 × 50.5 mm – half the size of a credit card) and lightweight (15.7 g). It can run for 2–4 years on 3×AA primary alkaline cells at 5 min logging intervals, and its hardware is rated to run from −40 to +85°C. Its firmware libraries (Schulz and Wickert, 2021a) mesh smoothly with the sensor APIs (Schulz and Wickert, 2020, 2022c). Its 18-bit ΣΔ analog–digital converter can read thermistors at 256× the resolution of the earlier ALog (Wickert, 2014; Wickert and others, 2019; Schulz, 2022) Data are stored in human-readable CSV files onto a swappable SD card.

Due to harsh polar and alpine weather conditions – including rime ice, snow, rain and condensing humidity – all electronics must be appropriately weatherproofed. Whereas the sensors are IP-67 rated, the data logger is not and so should be protected. We recommend a Polycase WH-04 enclosure, which is small (150 × 100 × 70 mm) but sufficient to hold the data logger and its batteries, as well as tightly sealing cable glands to link the data logger to the sensors (Fig. 4; Table 2) and desiccant packs.

2.4 Physical hardware

We recommend mounting the ultrasonic rangefinder at one end of an inverted U made of two 3/4" EMS conduit elbows held together with a compression coupling (Figs 2d,e; parts required in Table 2). This provides an easy way to securely hold this unit together in the field, while also permitting it to be broken down if needed for travel. To affix the ultrasonic rangefinder, we use a compression adapter that connects to a straight NPSM (National Pipe Straight Mechanical) connector. This can tighten down around the rangefinder with the aid of a lock nut and O ring. Wires pass down and out of the end of the U opposite the ultrasonic rangefinder, ensuring that water will not run down them and into the remainder of the apparatus (Fig. 4). If desired, this end may be sealed, either using cable glands and an appropriate compression adapter or a silicone sealant. We did not seal this end of the conduit U and encountered no problems. Using a pair of hose clamps (2.5–3.5-inch diameter: ~6.3–8.9 cm), we then affix this to the ablation stake.

Our ablation stake is a 2-inch (≈5 cm) outer diameter (OD) polyvinyl chloride (PVC) or high-density polyethylene (HDPE) pipe. This provides a smooth but snug fit into a hole bored vertically into the ice using Kovacs augers. Furthermore, PVC pipe is lightweight and thermally insulating relative to metal options, and this helps the field team bring it onto the glacier and prevents the stake from preferentially melting out of the ice. We recommend Schedule 80 pipe, as more rigid pipe helps to minimize sensor wobble as the ablation stake melts out. We are nonetheless concerned about the impact of these plastic ablation stakes on an otherwise pristine environment if they cannot be successfully recovered and have considered – though not yet implemented – environmentally degradable materials.

We install both the 'MaxTemp' temperature-compensation device for the ultrasonic rangefinder and the T9602 temperature and relative-humidity sensor into the solar radiation shield. This shield contains an inner screw-adjusted clamp that may be useful for at least one of these, but for reasons of speed and fit,

Figure 4. Materials to assemble the sensing component of the automated ablation stake. Lower left: Box with cable glands, Margay data logger and 3 ×AA battery pack. Upper left: 4× hose clamps. Upper right: Conduit inverted U with compression connector (top) and compression adapter (right); compression adapter threads onto the straight connector (far right) to attach to the MaxBotix ultrasonic rangefinder (lower right). Above middle: cable ties. Center (black cable): Temperature and relative-humidity sensor. Center right (gray cable): Cable to attach the MaxBotix ultrasonic rangefinder to the data logger. Lower middle: Solar radiation shield. Not pictured: MaxTemp temperature correction for the ultrasonic rangefinder; mounting hardware for the ultrasonic rangefinder.

Table 2. Component list

Item	QTY	Supplier	Part number	Purpose and/or description	Price[a]
3/4'' 90° EMT conduit elbow	2	McMaster–Carr	8081K12	Suspend ultrasonic rangefinder from ablation stake	8.62
3/4'' conduit compression connector	1	McMaster–Carr	7150K78	Connect two EMT elbow pieces	3.59
3/4'' conduit compression adapter	1	McMaster–Carr	7150K72	Connect ultrasonic rangefinder to EMT elbow	3.15
3/4'' NPSM straight connector	1	McMaster–Carr	7755K22	Connect ultrasonic rangefinder to EMT elbow	2.10
2.5–3.5'' hose clamps	4	McMaster–Carr	5407K24	Connect rangefinder assembly and logger box to main mast	15.74
1.5'' nominal (1.9'' OD) Schedule 80 PVC pipe[b]	1	McMaster–Carr	48855K15	Ablation stake main mast; priced for 10 feet (∼3 m)	43.60
Cable ties	8	McMaster–Carr	70215K65	Quantity estimated. For securing sensors in solar radiation shield and securing cabling. Black for UV resistance.	2.78
MaxBotix mounting hardware	1	MaxBotix	MB7950	3/4" lock nut and two O-rings	3.45
Ultrasonic rangefinder	1	MaxBotix	MB7388	Measure distance to ice or snow surface	137.94
MaxBotix Helper board	1	OSH Park	Custom[c,d]	Streamline wiring to the ultrasonic rangefinder	0.72
7-pin short male header block	1	Digi-Key	TSW-107-06-T-S	Connect MaxBotix Helper to ultrasonic rangefinder	0.76
Screw terminal block	1	Digi-Key	OSTVN06A150	Connect cables to MaxBotix Helper	1.86
Temperature correction	1	MaxBotix	MB7958[e]	HR-MaxTemp: Range correction for the speed of sound in air	34.44
Rangefinder cable	1	WesBell Elec.	ALP 5004C	3 m Alpha Wire 5004C: cut, stripped, and tinned	18.79
Temperature and relative humidity sensor	1	Digi-Key	T9602-3-D-1	Amphenol Telaire T9602: Measure drivers of ablation	55.10
Solar radiation shield	1	Dwyer	Series RHRS 6-plate[f]	Accurate temperature and relative-humidity measurements, including the MaxBotix temperature correction	50.50
1/4'' lock washer	2	McMaster–Carr	95584A207	External tooth; mount radiation shield to ablation-stake mast	0.04
1/4''×20 nut	2	McMaster–Carr	92673A113	Mount radiation shield to ablation-stake mast	0.07
Data Logger	1	Northern Widget[g]	Margay v2.2	Operate sensors and record data	200.00
Battery case	1	McMaster–Carr	7712K313	3×AA	2.85
Batteries	3	Battery Junction	MN1500	AA batteries to run logger and sensors	2.85
Enclosure[h]	1	PolyCase	WH-04	Outdoor-rated: Polycarbonate with clear lid	29.18
Cable glands	2	ElecDirect	RDC07AA	Gasketed cable pass-throughs from data logger to ultrasonic rangefinder and temperature & relative-humidity sensor	0.57
Total component cost					686.93

[a] US$ in year 2022 and given at the quantity required to build one system or the minimum order quantity, whichever is smaller.

[b] 48–50 mm OD PVC also works; the target outer diameter is 2". Items to stabilize the main mast are not included because we have not fully researched what the best option may be.

[c] Use CAD files from Wickert (2019).

[d] Although an inclinometer can be helpful, incorporating one would require including and/or designing a new circuit board, which is not part of the present design. We would recommend modifying the MaxBotix-Helper (Wickert, 2019) to include the integrated ATTiny microcontroller, STM and STMicroelectronics LIS3DHTR, with a firmware-enabled I^2C interface (following Schulz, 2019).

[e] Other HR-MaxTemp options are available that are less expensive and not fully assembled.

[f] Yellows and becomes brittle with UV exposure.

[g] Design is also available open source (Schulz and Wickert, 2021b).

[h] Not listed here are optional and/or custom items used with the enclosure, including adhesives and/or fasteners to secure the logger and batteries and desiccant packs.

we typically secure one or both into the housing using cable ties. Proper ventilation of such a shield is important, especially under windless and clear-sky conditions. Passively ventilated shields such as the one that we use experienced excess heating of 0.3–1.3°C (Cordillera Blanca, Peru: Georges and Kaser, 2002) and up to 8°C (East Antarctic Plateau Morino and others, 2021) when compared to mechanically ventilated shields. While these passive shields have advantages in simplicity and power requirements, care must be taken to ensure that effective passive ventilation can take place.

Following this, we attach both the solar radiation shield and the data-logger box to the 2-inch PVC pipe in a location that is out of the path of the ultrasonic rangefinder. For the data-logger box, we employ these same 2.5–3.5 inch hose clamps; smaller hose clamps could be used, but we find it best to limit the number of unique parts required when managing field-deployment logistics, especially when two can look similar and may be confused during field preparations. These are run through slots in the metal 'feet' of the data-logger box and cinched down around the PVC ablation-stake mast. The recommended solar radiation shield comes with its own 2-inch U bolt, which includes a rubberized component that adds friction and is ideal for the 2-inch PVC pipe ablation-stake mast. Its lock nuts are slow and difficult to use in the field, so we recommend that users bring separate 1/4"–20 nuts and lock washers as indicated in Table 2.

We secure any slack from cables to the data-logger main mast, out of the way of the ~0.3 m sensing radius of the ultrasonic rangefinder. Electrical cables can easily blow in the strong winds common on glaciers while simultaneously becoming more brittle due to UV damage. This combination can cause them to break, making it imperative to properly secure them.

2.5 Installation and maintenance

We install the automated ablation stake by drilling a hole using Kovacs ice augers, ensuring both that it is vertical and that its depth will keep the rangefinder beyond its minimum range (0.5 m for the MB7388) from the ice surface. We then insert the PVC pipe into this hole while packing excess ice shavings around it; adding these and water helps to freeze the ablation stake in place.

A design using just a single pole is relatively lightweight, but is more likely to bend as melting exposes a taller mast and can be prone to rotation in the wind. To avoid problems related to bending, we used thicker and more rigid plastic pipe and – in some of our designs – included an inclinometer to detect and correct for a non-vertical sensor. To address both of these problems, we suggest that installations when possible be made in flat areas of the ice surface. Furthermore, we secured the ablation stakes on Glaciar Fourcade (Fig. 2e) with three staked guy wires, which we adjusted and re-staked during data-download visits (2–3 times per week). An alternative option is to build a more stable platform with multiple masts extending into the glacier surface, as we had on Kennicott Glacier (Armstrong and Anderson, 2020) (Figs 2a,b), though a more stable set-up could include farther-spaced masts (e.g. Oerlemans, 2000; Munro and others, 2004) to prevent the net twisting noticeable between Figures 2a and b.

Maintaining battery life requires knowledge of power consumption and equipment used. The most recent deployments employ Margay data loggers (Schulz and Wickert, 2021b), which draw 1.3 μA (quiescent) and 8.6 mA (active). When active, the sensors require 2.9 mA (MaxBotix rangefinder) and 0.750 mA (T9602 temperature and relative-humidity sensor); considering the usage of the additional temperature sensor (MaxTemp) and rounding up for safety, the active current draw is ≤13 mA. Considering a conservative AA battery capacity of 2000 milliamp-hours, one reading per 5 min, and a sampling time of 2 s, the device should last for approximately 2.5 years.

Upon each installation and site visit, one should take local measurements as ground truth and perform maintenance: (1) Measure and record the distance from a marked point on the ablation stake – either the rangefinder sensing element or something that is offset a known distance from this – to the snow/ice surface. (2) Note and photograph the state of the stake and ground surface, including information on snow vs ice cover, any damage to the stake, and tilt or excessive melt or wind scour (or shielding from melt) around the mast. (3) Record the coordinates of the stake; this can be useful additional information for ice velocity and for finding the stake again on a moving glacier; such positioning information comes alongside a timestamp, as should photos, and this can help to filter bad data, including rangefinder returns off of humans standing on the ice. (4) If the data logger can be reached, download and/or swap its data-storage device. Sometimes ablation stakes disappear. (5) Replace the batteries if needed. (6) Move and reinstall the ablation stake if it seems unstable; record if and when this has been done.

3. Temperature-index melt modeling

The critical advantage of having co-located and high-resolution temperature and ablation data lies in the opportunity to calibrate, probe and expand well-established temperature-index modeling approaches (e.g. Braithwaite and Olesen, 1989; Hock, 2003). Each automated ablation stake provides its own self-contained calibration site for a temperature–ablation relationship. The frequent data allow us to investigate different methods and time windows over which to estimate the 'melt factor', which relates temperature to ablation rate, and to explore systematic variations in its value. Indeed, Hock (2003) notes the importance of such highly time-resolved data to avoid averaging across temperatures above and below T_0.

Although each ablation stake is self-sufficient, every deployment pictured in Figure 2 employed ~3 ablation stakes per glacier (Wickert and others, 2023) to account for potential local variability in melt rate (Braithwaite, 2008) and to ensure redundancy in the case of equipment failure. When deployed along an elevation transect, these multiple ablation stakes can also record the on-ice temperature lapse rate (Romero and others, 2022), which can aid mass-balance modeling (cf. Anderson and others, 2014).

3.1 Temperature-index models and melt factors

A typical temperature-index ablation model has the form (partially following variable nomenclature from Hock, 2003):

$$\dot{\mathcal{A}} = \begin{cases} f_{\mathrm{m}}(T - T_0) & \text{if } T > T_0 \\ 0 & \text{otherwise} \end{cases}. \quad (1)$$

Here, $\dot{\mathcal{A}}$ is ablation rate [mm w.e. d^{-1}]; f_{m} is a 'melt factor' [mm w.e. $°C^{-1}$ d^{-1}], which linearly scales temperature to ablation rate (and is a slight misnomer because ablation may include sublimation in addition to melt); T is the air temperature; and T_0 is the air temperature at which ablation begins. When T_0 is zero, f_{m} may also be called the degree-day factor (DDF), and this equation may be called a 'positive-degree-day' (PDD) ablation model. To create a variable representing the temperature used in such a PDD model, we define T^+, the 'positive temperature' to be equal to the temperature when above the freezing point and 0 when at or below the freezing point,

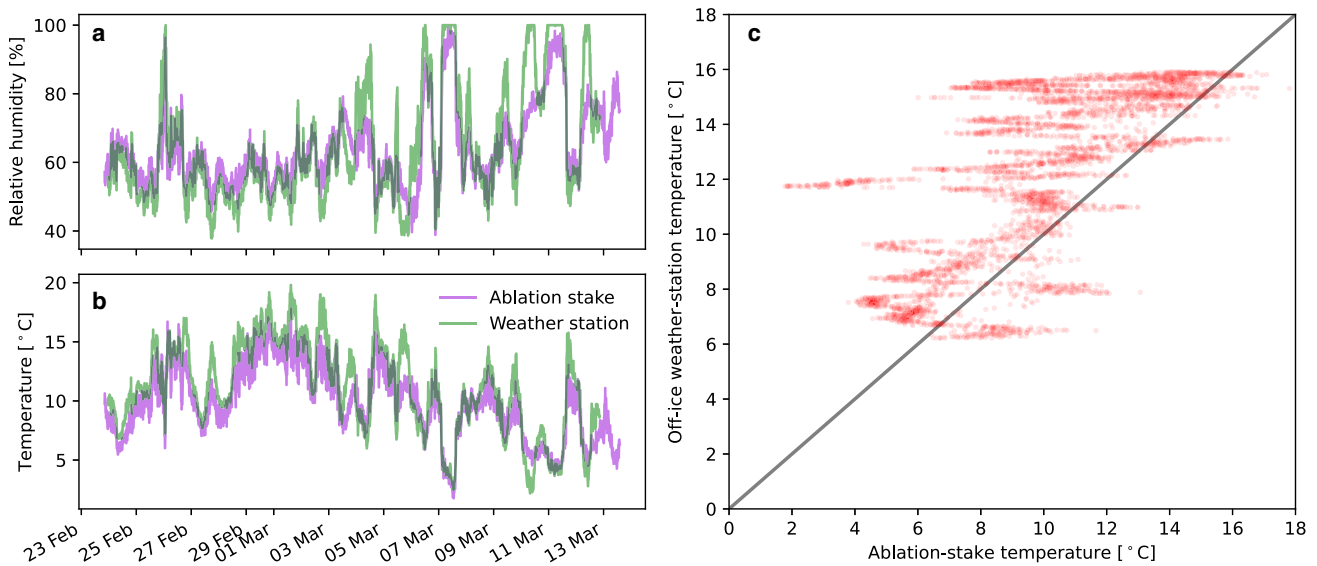$$T^+ = \begin{cases} T & \text{if } T > 0 \\ 0 & \text{otherwise} \end{cases}. \quad (2)$$

Figure 5. **(a)** Relative-humidity and **(b)** temperature records from the ablation stake demonstrated here (AS-1; 50.5162°S, 73.1280°W) and the nearby weather station that we installed (WS-2: Buscaini; 50.51844°S, 73.12766°W). **(c)** Off-ice temperatures are generally higher and more variable (see panel b) than those in the supraglacial boundary layer. The gray line denotes unity. Data are from the year 2020.

Despite the common use of temperature-index melt models, a range of both averaging times (typically one day, though this may be hourly to monthly) and measurement periods (a few days to several years) have been used to obtain f_m, thereby making inter-comparison among studies difficult (Hock, 2003). Here we demonstrate the utility of the automated ablation stakes by applying data from one installation – on Glaciar Perito Moreno,

Argentina – to address and develop methods to approach melt-factor calculation and temperature-index model generation.

3.2 Data: Perito Moreno

As an example implementation of these automated ablation stakes, we present data from a February–March 2020 ablation-
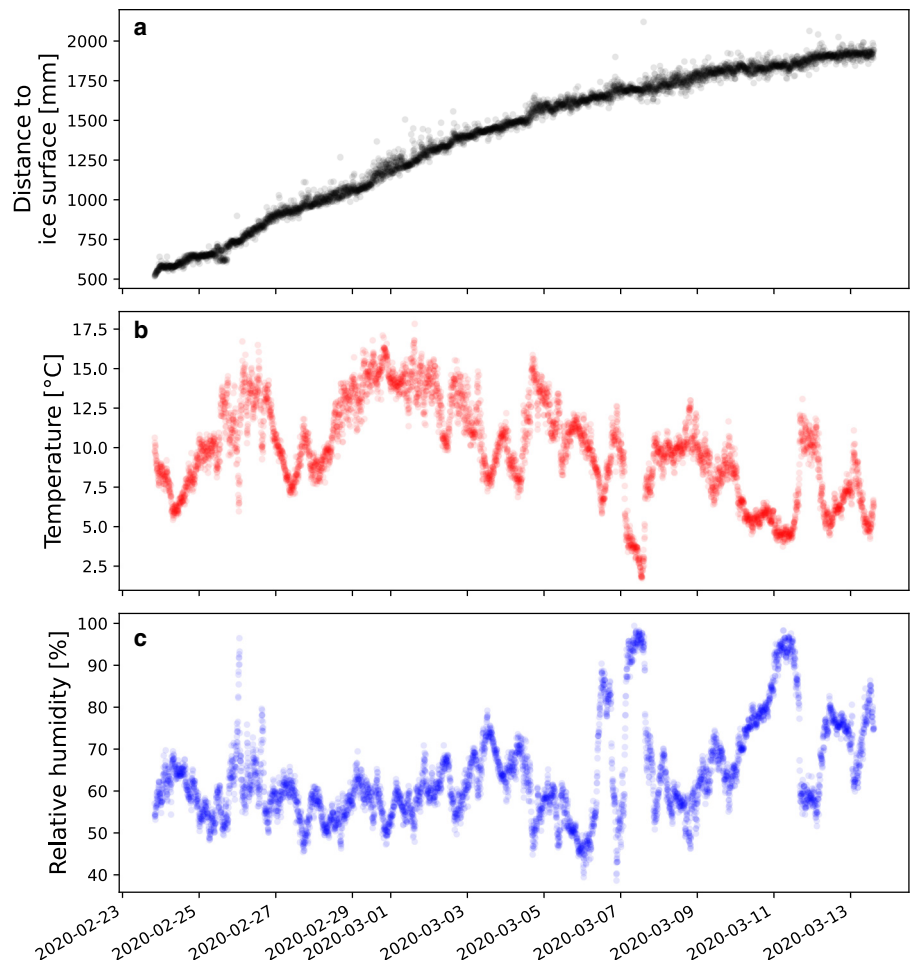
Figure 6. Measured ice-surface elevation, atmospheric temperature and relative humidity on Glaciar Perito Moreno, Argentina, from late February to mid March, 2020. The ablation stake was installed near the southern margin of the glacier. (a) Distance to the ice surface nearly monotonically increases, indicating persistent and near-continuous ablation without the complication of snow cover. (b) Temperatures are nearly entirely above the freezing point during the measurement period. (c) Relative humidity increases during times of cooling due to the decreased saturation vapor pressure of air.

stake installation near the southern margin of Glaciar Perito Moreno, Patagonia, Argentina (Stake AS-1 out of three stakes total; Figs 2d, 6). We installed this ablation stake on a prominent and locally flat surface within this heavily crevassed region of ice. Distance to the ice surface, atmospheric temperature and atmospheric relative humidity were measured and recorded every 5 min, and raw data are available from Wickert and others (2023).

Additionally, we established a weather station immediately off-ice from these ablation stakes (Van Wyk de Vries and others, 2022; Wickert and others, 2022), whose measurements of temperature and relative humidity are consistent those measured at the automated ablation stakes (Fig. 5). Importantly, these measurements include wind speeds, which average to $0.6 \, \text{m s}^{-1}$ and therefore indicate sufficient ventilation of the temperature and relative
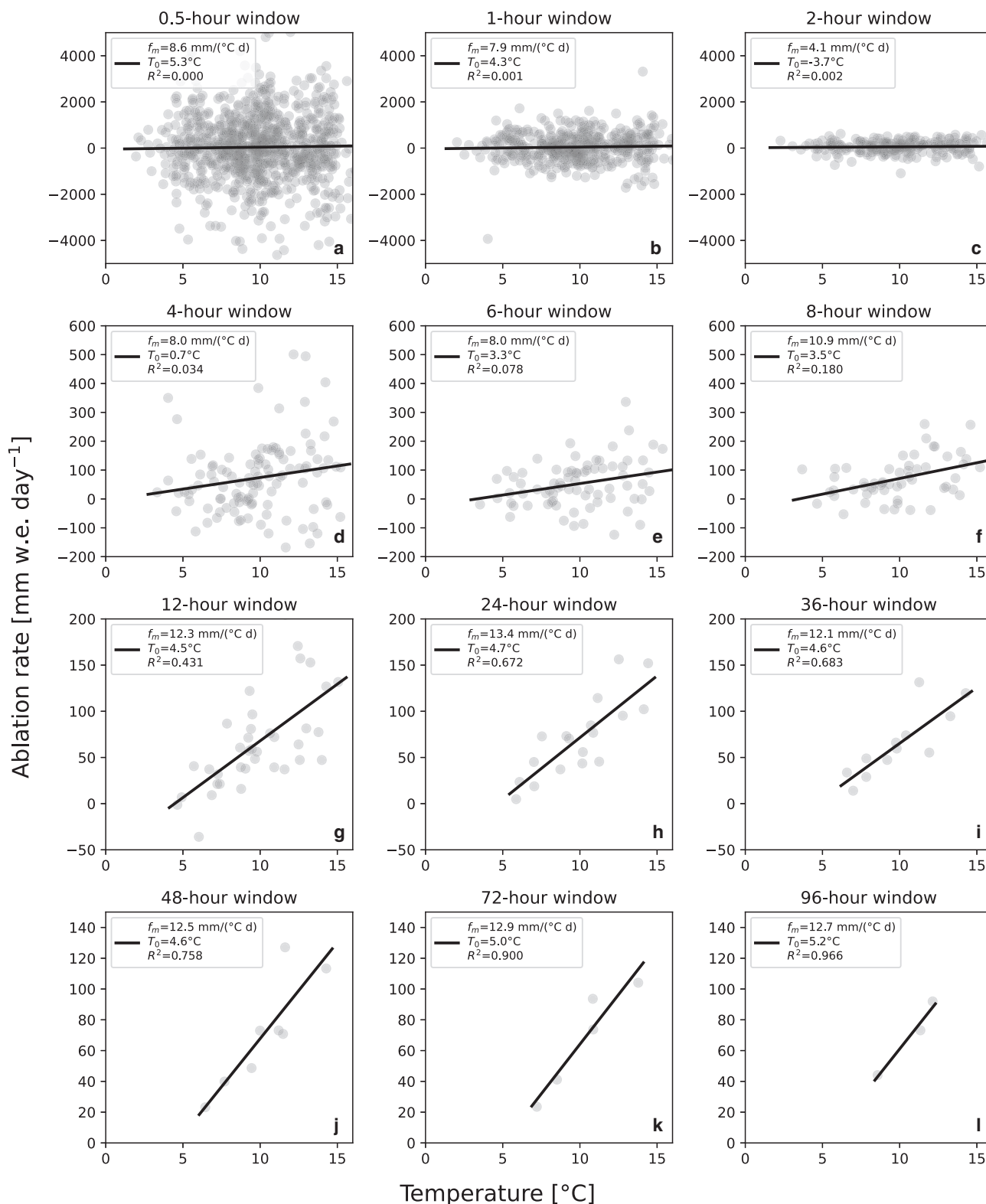
Figure 7. Melt-factor (f_m) and melt-threshold-temperature (T_0) calculations using a linear regression between temperature and ablation rate. Within each averaging window, we compute the mean temperature and an ablation rate calculated via a linear regression between distance to the ice surface, obtained from the ultrasonic rangefinder, and time.

humidity sensors. For contextual information on Glaciar Perito Moreno and its mass balance, see Stuefer and others ([2007](#)) and Minowa and others ([2023](#)).

The Perito Moreno AS-1 dataset exhibits approximately monotonically increasing distance to the ice surface, indicating persistent ablation without accumulation, alongside temperatures that are always $> 0°C$ (Fig. 6). Both factors streamline data interpretation. To convert ablation distances into water-equivalent loss, we follow Stuefer and others ([2007](#)) in assuming an ice density of $900 \, \text{kg m}^{-3}$.

3.3 Estimating the melt factor, f_m

We estimate f_m using three methods. First, we compute total melt and PDDs (following Braithwaite and Olesen, [1989](#); Braithwaite, [2008](#)) to calculate a melt factor representative of the full observed period. In the second, we compute a linear regression between daily melt rate and daily temperature (cf. Howat and others, [2007](#)). Our third method is a discrete integration to compare net ablation to total PDDs, taking advantage of the high temporal resolution of the data supplied by the automated ablation stake.

3.3.1 Total ablation

We divide the total amount of ablation – calculated as the difference in mean ice-surface elevation between the initial and final hours of the deployment – by the total positive degree days during the deployment. From this, we obtain $f_m = 1256 \, \text{mm w.e.}/(9.8°C \cdot 18.7\text{d}) = 6.8 \, \text{mm w.e.} \, °C^{-1} \, d^{-1}$. This value is lower than the $7.4 \, \text{mm w.e.} \, °C^{-1} \, d^{-1}$ mean rate found for Austral summer ablation in similarly crevassed, ice-marginal areas of Glaciar Perito Moreno, though there was significant scatter among the individual stake measurements (Stuefer and others, [2007](#)). It lies well within the $7.3 \pm 2.7 \, \text{mm w.e.} \, °C^{-1} \, d^{-1}$

mean and standard deviation of DDF values compiled from 92 individual measurement sites worldwide (Brugger and others, [2021](#)).

3.3.2 Ablation rate vs temperature

We follow Eqn ([1](#)) to compute f_m and T_0. Within a given time window, we compute average melt rate through a linear regression of distance from the ultrasonic rangefinder to the ice surface with time. Over this same time window, we compute the mean temperature. We then perform a second linear regression, this time of melt rate vs temperature, to compute f_m and T_0 (following Eqn ([1](#))).

Using the 5 min data from Glaciar Perito Moreno, we repeated this calculation over time windows ranging from 30 min to 4 d (Fig. 7). We performed no filtering or outlier removal prior to these fits, and their quality represents the combined effects of (a) instrumental accuracy and precision and (b) physical grounds for the correlation. Both f_m and T_0 converged to consistent values for averaging times $\gtrsim 12 \, \text{h}$ (Fig. 8), in agreement with the diurnal cycle in melt factor, forced by solar radiation, noted by Singh and Kumar ([1996](#)). R^2 increased throughout because of both this convergence and data averaging across longer windows. For time windows $\geq 12 \, \text{h}$, $f_m \approx 12.5 \, \text{mm w.e.} \, °C^{-1} \, d^{-1}$ and $4.5 \lesssim T_0 \lesssim 5.2 \, °C$. The unusually high values for both T_0 and f_m are artifacts of our data series, in which time-resolved f_m decreases (Fig. 9) as temperature also drops. In contrast, the degree-day factor (DDF) – that is, the melt factor when T_0 is set to $0°C$ – for the commonly used 1 d averaging window (Hock, [2003](#)) is $7.6 \, \text{mm w.e.} \, °C^{-1} \, d^{-1}$; here, $R^2 = 0.53$ (Fig. 9a).

3.3.3 Integral approach

We take advantage of our 5 min data to build a discrete integral of total positive-degree days to compare against the total amount of
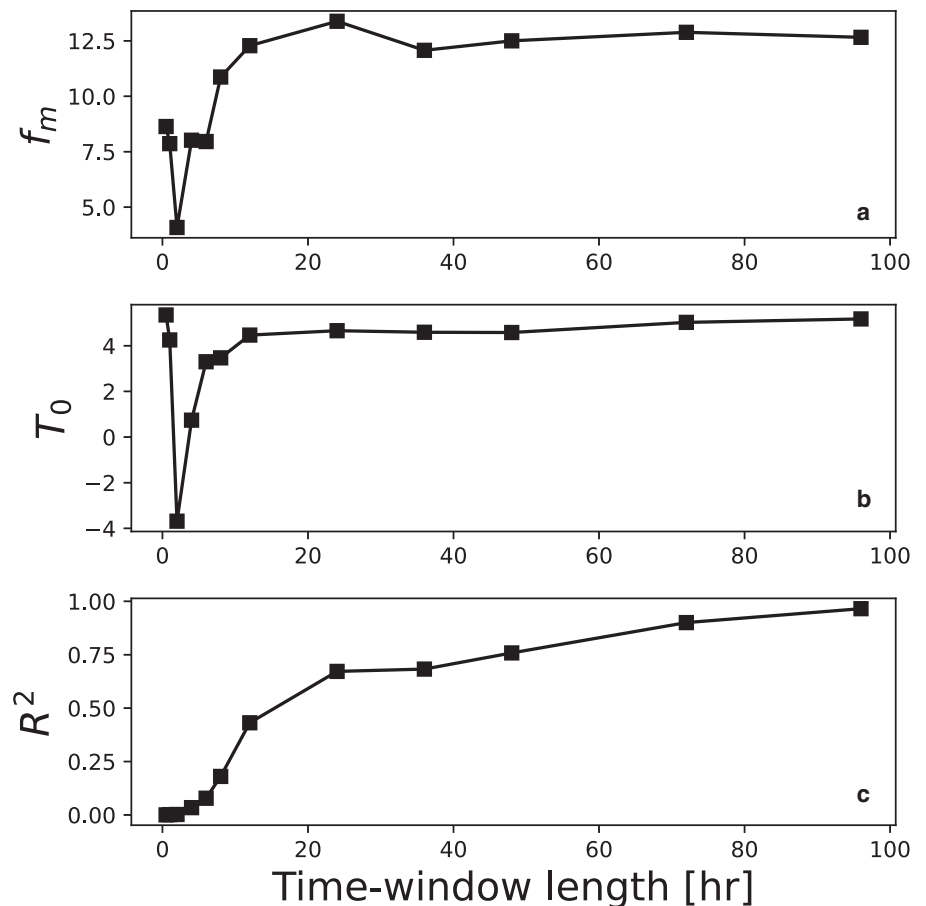

Figure 8. Temperature-index fit parameters as a function of time-window length. Each point corresponds to a subpanel plot of Figure 7. (a) Melt factor, f_m. (b) Temperature at which ablation begins, T_0. (c) Coefficient of determination, R^2. The parameters converge when measurements are averaged over 12 h.

ice-surface lowering:

$$\mathcal{A}_n = f_{\mathrm{m}} \sum_{i=1}^{n} T_i^{+} (\Delta t)_i. \qquad (3)$$

Here, $\mathcal{A}_n$ is the cumulative ablation from the start of the measurement time series until time t_n. Based on the mean ice-surface-lowering rate (3.15 mm h^{-1}) and the sensor precision (± 1 mm), these 5 min data should fully resolve ablation within instrumental precision.

Using Eqn (3), we compute a linear fit (Fig. 9b), which results in a DDF of 7.5 mm w.e. $^{\circ}$C^{-1} d^{-1}, with a coefficient of determination of $R^2 = 0.96$; this melt factor value is identical to that from the regression over daily data for which the temperature intercept is 0 (Fig. 9a). The closer fit between model and data is unsurprising because integral approaches sum and smooth random error. Furthermore, it is close to the DDF of 7.4 mm w.e. $^{\circ}$C^{-1} d^{-1} obtained by Stuefer and others (2007) on Glaciar Perito Moreno using a similar integral approach with frequently measured total ablation (their Fig. 6b). Although we do not perform such a calculation here, it is possible to apply this integral approach to find a nonzero T_0 alongside an associated f_{m}.

4. Discussion

4.1 Temperature-measurement height

The fixed position of the atmospheric sensors on the stake – inside the solar radiation shield – results in their elevations above the ice surface increasing as the glacier ablates. This contrasts with standard atmospheric monitoring deployments that are 2 m above the surface (e.g. Greuell and Böhm, 1998). Marshall and others (2007, pp. 388–389) systematically measured temperatures from 0.1 to 2.0 m above the surface at 0.1 m intervals, and found that sensors deployed above 0.5 m reported temperatures within 0.1 $^{\circ}$C of one another, though this may be vary with surface roughness and wind shear. Atmospheric sensors for the automated ablation stake are always installed 0.5 m above the ice surface because the solar radiation shield should be above the ultrasonic rangefinder, whose minimum ranging distance is 0.3–0.5 m. To maintain a constant temperature-sensor height above the ice surface in future designs, the temperature sensor could be mounted to maintain a constant height above the glacier surface – for example, on a PVC tube that slides freely down a thinner pole that is fixed into the ice (following Oerlemans, 2000), a platform that moves down with the melting glacier surface, or a pendulum-stabilized tripod that likewise lowers with the ice surface (Kaser and others, 2004).

4.2 On-ice measurements and the glacial boundary layer

Because the ablation-stake temperature sensor samples the air in the boundary layer above the ice surface, its readings may be affected by ice melt, sublimation, reflected radiation, and/or other mechanisms of ice–atmosphere energy exchange. This is a concern because Guðmundsson and others (2009) found that off-ice temperature data better represent the incoming solar radiation flux than do on-ice data, indicating that off-ice data could be more appropriate to drive temperature-index ablation models. Furthermore, such boundary-layer energy transfer may make the ablation-stake record distinct from those measured by off-ice stations or produced as outputs from downscaled atmospheric models. Both of the latter are used to drive temperature-index melt models.

To investigate this question in our test case, we compared the ablation-stake data against data recorded at the nearby off-ice weather station (WS-2: Buscaini) that we also installed
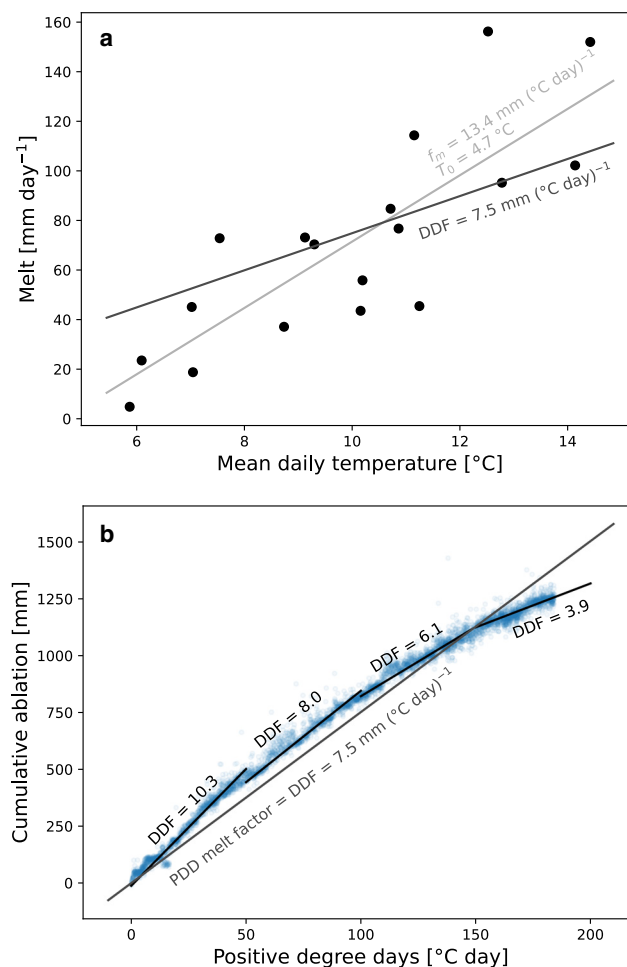

Figure 9. Melt-factor calculations. (a) Computation of melt factors using a regression between temperatures and daily melt rates. DDF: positive-degree-day melt factor. Intercept at $T = 0$ (i.e. $T_0 = 0$ $^{\circ}$C; DDF calculated): $R^2 = 0.52$. Intercept allowed to vary (i.e. f_{m} calculated): $R^2 = 0.69$. (b) Melt-factor calculation via an integral approach (Eqn 3). $R^2 = 0.96$ for the linear regression on the full dataset, which includes a systematic bias in the residuals. Data-subset fits beginning (arbitrarily) every 50 positive degree days produce degree-day factors that decrease systematically from 10.3 to 3.9 mm w.e. $^{\circ}$C^{-1} d^{-1}.

(Wickert and others, 2022). We note strong similarity in both temperature and relative humidity between these on-ice and off-ice data (Fig. 5). For the period over which both on- and off-ice data exist, $f_{\mathrm{m}} = 7.3$ mm w.e. $^{\circ}$C^{-1} d^{-1} using the on-ice data and $f_{\mathrm{m}} = 6.5$ mm w.e. $^{\circ}$C^{-1} d^{-1} using the off-ice data, both using the integral approach. The higher f_{m} for the ablation-stake temperature record reflects the lower average air temperature above the glacier than at the off-ice weather station. The curved systematic departure from a linear ablation–PDD fit (Fig. 9) persisted regardless of whether on-ice or off-ice temperature data were used.

4.3 Deviation from a constant DDF

Despite the high R^2 value shown using the integral approach (Fig. 9b), the data systematically trend off of the linear fit. By splitting the time series into four bins, starting each 50 degree days, we demonstrate a monotonic decrease in DDF from 10.3 mm w.e. $^{\circ}$C^{-1} d^{-1} at the beginning of the time series to 3.9 mm w.e. $^{\circ}$C^{-1} d^{-1} at its end. These fall within the range of ice DDF estimates compiled by Brugger and others (2021), though the 3.9 mm w.e. $^{\circ}$C^{-1} d^{-1} would be the second-lowest value of those that they found in the literature. In contrast to our findings, Stuefer and others (2007, Fig. 6b) found a very

strong linear fit for their degree-day factor (DDF = 8.8 mm w.e. $^{\circ}C^{-1}$ d^{-1}; R^2 = 0.997; T_0 fixed at 0 °C) without any noticeable residual; this ablation stake was installed in the same region of Glaciar Perito Moreno, and Stuefer and others (2007) used a similar integral approach to compute the melt factor.

A few possibilities emerge for the reason behind this decrease in DDF. First, the temperature and humidity records (Fig. 5) suggest a shift to stormier conditions in March. This could indicate a shift from radiation-dominated to sensible-heat-dominated ablation. Sensible-heat effects produce a smaller melt factor and have been previously noted at Glaciar Perito Moreno (Takeuchi and others, 1995; Minowa and others, 2023). Second, field photos of our deployment indicate that the measured ice surface sloped toward the equator at first but, as it melted, later sloped toward the pole (Supplementary Fig. 1). This would reduce received solar radiation over time. Third, this change in ice-surface slope might have affected the ultrasonic rangefinder measurements. Finally, we note that our data extend over <200 PDDs whereas the much more linear Stuefer and others (2007) dataset extends across 1400 PDDs. A longer measurement time series could average over the shorter-term variability in whether solar radiation or sensible heat fluxes more strongly drive temperature and ablation (cf. Ohmura, 2001; Minowa and others, 2023).

5. Conclusion

We developed, tested and improved automated ablation stakes over a decade. These automated ablation stakes enable us to generate calibrated ablation models based on frequent and co-located data on relative ice-surface-elevation change and atmospheric drivers of ablation, with the present design suited for temperature-index approaches. Their autonomous data recording and low power requirements enable high temporal resolution, and their low cost and portability facilitate large-scale deployments. Aside from the sensors themselves, the ablation-stake design, hardware and firmware are open source. Table 2 contains our recommended parts list alongside suggestions for future installations.

Through analysis of a test deployment in Patagonia, we evaluate methods for computing temperature-index melt factors. When fitting a linear regression to temperature and ablation rate, parameters f_m and T_0 converge as averaging windows exceed ~12 h. The integral approach, made possible by the frequent data, improves goodness of fit while exposing a systematic residual. Future deployments using this automated ablation-stake technology should aid efforts to link ablation to drivers of glacier-surface mass loss.

References

Andermann C and 5 others (2012) Impact of transient groundwater storage on the discharge of Himalayan rivers. *Nature Geoscience* **5**(2), 127–132. doi: 10.1038/ngeo1356

Anderson LS, Roe GH and Anderson RS (2014) The effects of interannual climate variability on the moraine record. *Geology* **42**(1), 55–58. doi: 10.1130/G34791.1

Armstrong WH and Anderson RS (2020) Ice-marginal lake hydrology and the seasonal dynamical evolution of Kennicott Glacier, Alaska. *Journal of Glaciology* **66**(259), 699–713. doi: 10.1017/jog.2020.41

Beddows PA and Mallon EK (2018) Cave pearl data logger: a flexible Arduino-based logging platform for long-term monitoring in harsh environments. *Sensors (Switzerland)* **18**(2), 530. doi: 10.3390/s18020530

Braithwaite RJ (2008) Temperature and precipitation climate at the equilibrium-line altitude of glaciers expressed by the degree-day factor for melting snow. *Journal of Glaciology* **54**(186), 437–444. doi: 10.3189/002214308785836968

Braithwaite RJ and Olesen OB (1989) Calculation of glacier ablation from air temperature, West Greenland. In Oerlemans J ed. *Glacier Fluctuations and Climatic Change*, Glaciology and Quaternary Geology, 219–233, Springer Dordrecht, doi: 10.1007/978-94-015-7823-3_15.

Braun LN, Escher-Vetter H, Heucke E, Siebers M and Weber M (2004) Experiences with the new hydro-meteorological station Vernagtbach. In *Automated Weather Stations on Glaciers*, Institute for Marine and Atmospheric Research Utrecht, Pontresina, Switzerland, 38–44.

Brook MS and Paine S (2012) Ablation of ice-cored moraine in a humid, maritime climate: Fox glacier, New Zealand. *Geografiska Annaler, Series A: Physical Geography* **94**(3), 339–349. doi: 10.1111/j.1468-0459.2011.00442.x

Brugger KA, Leonard EM, Refsnider KA and Dolan P (2021) Climate on the Blanca Massif, Sangre de Cristo Mountains, Colorado, USA, during the Last Glacial Maximum. *Quaternary* **4**(3), 27. doi: 10.3390/quat4030027

Carenzo M, Pellicciotti F, Rimkus S and Burlando P (2009) Assessing the transferability and robustness of an enhanced temperature-index glacier-melt model. *Journal of Glaciology* **55**(190), 258–274. doi: 10.3189/002214309788608804

Deline P and 16 others (2021) Chapter 15 – ice loss from glaciers and permafrost and related slope instability in high-mountain regions. In Haeberli W and Whiteman C eds. *Snow and Ice-Related Hazards, Risks, and Disasters (2nd Ed.)*, Hazards and Disasters Series, 501–540, Elsevier, Amsterdam, doi: 10.1016/B978-0-12-817129-5.00015-9

Ensign S and 6 others (2019) A digital mayfly swarm is emerging. *Eos* **100**, doi: 10.1029/2019EO116611

Evans NT (2016) *Assessing hydrologic connectivity using water temperature, Wax Lake Delta, Louisiana*. Ph.D. thesis, University of Minnesota, Minneapolis, MN, USA.

Fausto RS and 16 others (2021) Programme for Monitoring of the Greenland Ice Sheet (PROMICE) automatic weather station data. *Earth System Science Data* **13**(8), 3819–3845. doi: 10.5194/essd-13-3819-2021

Gabbud C, Micheletti N and Lane SN (2015) Instruments and methods: Lidar measurement of surface melt for a temperate Alpine glacier at the seasonal and hourly scales. *Journal of Glaciology* **61**(229), 963–974. doi: 10.3189/2015JoG14J226

Georges C and Kaser G (2002) Ventilated and unventilated air temperature measurements for glacier-climate studies on a tropical high mountain site. *Journal of Geophysical Research: Atmospheres* **107**(D24), ACL 15-1–ACL 15-10. doi: 10.1029/2002JD002503

Greuell W and Böhm R (1998) 2 m temperatures along melting mid-latitude glaciers, and implications for the sensitivity of the mass balance to variations in temperature. *Journal of Glaciology* **44**(146), 9–20. doi: 10.3189/S0022143000002306

Guðmundsson S, Björnsson H, Pálsson F and Haraldsson HH (2009) Comparison of energy balance and degree-day models of summer ablation on the Langjökull ice cap, SW-Iceland. *Jökull* **59**, 1–18. doi: 10.33799/jokull2009.59.001

Gunnarsson A, Gardarsson SM, Pálsson F, Jóhannesson T and Sveinsson ÓGB (2021) Annual and inter-annual variability and trends of albedo of Icelandic glaciers. *The Cryosphere* **15**(2), 547–570. doi: 10.5194/tc-15-547-2021

Gusain H, Singh K, Mishra V, Srivastava P and Ganju A (2009) Study of surface energy and mass balance at the edge of the Antarctic ice sheet during summer in Dronning Maud Land, East Antarctica. *Antarctic Science* **21**(04), 401. doi: 10.1017/S0954102009001989

Hagg W, Mayer C, Lambrecht A and Helm A (2008) Sub-debris melt rates on southern Inylchek Glacier, Central Tian Shan. *Geografiska Annaler: Series A, Physical Geography* **90**(1), 55–63. doi: 10.1111/j.1468-0459.2008.00333.x

Hay CC, Morrow E, Kopp RE and Mitrovica JX (2012) Fostering advance in interdisciplinary climate science Sackler Colloquium: estimating the sources of global sea level rise with data assimilation techniques. *Proceedings of the National Academy of Sciences* **110**, 3692–3699. doi: 10.1073/pnas.1117683109

Hock R (1999) A distributed temperature-index ice- and snowmelt model including potential direct solar radiation. *Journal of Glaciology* **45**(149), 101–111. doi: 10.3189/S0022143000003087

Hock R (2003) Temperature index melt modelling in mountain areas. *Journal of Hydrology* **282**(1–4), 104–115. doi: 10.1016/S0022-1694(03)00257-9

Hock R and Holmgren B (2005) A distributed surface energy-balance model for complex topography and its application to Storglaciären, Sweden. *Journal of Glaciology* **51**(172), 25–36. doi: 10.3189/172756505781829566

Howat IM, Tulaczyk S, Rhodes P, Israel K and Snyder M (2007) A precipitation-dominated, mid-latitude glacier system: Mount Shasta, California. *Climate Dynamics* **28**(1), 85–98. doi: 10.1007/s00382-006-0178-9

Hulth J (2010) Using a draw-wire sensor to continuously monitor glacier melt. *Journal of Glaciology* **56**(199), 922–924. doi: 10.3189/002214310794457290

Immerzeel WW and 6 others (2014) High-resolution monitoring of Himalayan glacier dynamics using unmanned aerial vehicles. *Remote Sensing of Environment* **150**, 93–103. doi: 10.1016/j.rse.2014.04.025

Jacob T, Wahr J, Pfeffer WT and Swenson S (2012) Recent contributions of glaciers and ice caps to sea level rise. *Nature* **482**(7386), 514–518. doi: 10.1038/nature10847

Karpilo Jr RD (2009) Glacier monitoring techniques. In Young R and Norby L eds. *Geological Monitoring*, 141–162, Geological Society of America, doi: 10.1130/2009.monitoring(06).

Kaser G, Irmgard J and Giegele T (2004) An AWS mounting device which mechanically adjusts itself to changing glacier surface conditions. In *Automated Weather Stations on Glaciers*, Institute for Marine and Atmospheric Research Utrecht, Pontresina, Switzerland, 59–62.

Keeler ML and Brugger KA (2012) A method for recording ice ablation using a low-cost ultrasonic rangefinder. *Journal of Glaciology* **58**(209), 565–568. doi: 10.3189/2012JoG11J153

Kochanski K, Anderson RS and Tucker GE (2019) The evolution of snow bedforms in the Colorado Front Range and the processes that shape them. *The Cryosphere* **13**(4), 1267–1281. doi: 10.5194/tc-13-1267-2019

Labine C and Koerner RF (2004) Autostations networks in the Canadian Arctic Archipelago: twenty years later, issues and problems. In *Automated Weather Stations on Glaciers*, Institute for Marine and Atmospheric Research Utrecht, Pontresina, Switzerland, 66–71.

La Frenierre J and Mark BG (2014) A review of methods for estimating the contribution of glacial meltwater to total watershed discharge. *Progress in Physical Geography* **38**(2), 173–200. doi: 10.1177/0309133313516161

Landmann JM and 5 others (2021) Assimilating near-real-time mass balance stake readings into a model ensemble using a particle filter. *The Cryosphere* **15**(11), 5017–5040. doi: 10.5194/tc-15-5017-2021

Larour E, Ivins ER and Adhikari S (2017) Should coastal planners have concern over where land ice is melting? *Science Advances* **3**(11), 1700537. doi: 10.1126/sciadv.1700537

Litt M and 6 others (2019) Glacier ablation and temperature indexed melt models in the Nepalese Himalaya. *Scientific Reports* **9**(1), 5264. doi: 10.1038/s41598-019-41657-5

MacDonell S, Kinnard C, Mölg T, Nicholson L and Abermann J (2013) Meteorological drivers of ablation processes on a cold glacier in the semi-arid Andes of Chile. *The Cryosphere* **7**(5), 1513–1526. doi: 10.5194/tc-7-1513-2013

Machguth H, Paul F, Hoelzle M and Haeberli W (2006) Distributed glacier mass-balance modelling as an important component of modern multi-level glacier monitoring. *Annals of Glaciology* **43**, 335–343. doi: 10.3189/172756406781812285

Marshall SJ, Sharp MJ, Burgess DO and Anslow FS (2007) Near-surface-temperature lapse rates on the Prince of Wales Icefield, Ellesmere Island, Canada: implications for regional downscaling of temperature. *International Journal of Climatology* **27**(3), 385–398. doi: 10.1002/joc.1396

Meier MF (1969) Glaciers and water supply. *Journal AWWA* **61**(1), 8–12. doi: 10.1002/j.1551-8833.1969.tb03696.x

Meier MF and 7 others (2007) Glaciers dominate eustatic sea-level rise in the 21st century. *Science* **317**(5841), 1064–1067. doi: 10.1126/science.1143906

Minowa M, Skvarca P and Fujita K (2023) Climate and surface mass balance at glaciar perito moreno, Southern Patagonia. *Journal of Climate* **36**(2), 625–641. doi: 10.1175/JCLI-D-22-0294.1

Morino S and 9 others (2021) Comparison of ventilated and unventilated air temperature measurements in Inland Dronning Maud Land on the East Antarctic Plateau. *Journal of Atmospheric and Oceanic Technology* **38**(12), 2061–2070. doi: 10.1175/JTECH-D-21-0107.1

Munro DS, Demuth MN and Moore D (2004) Operating the AWS at Western Canada Glacier Sites. In *Automated Weather Stations on Glaciers*, Institute for Marine and Atmospheric Research Utrecht, Pontresina, Switzerland, 72–75.

Netto GT and Arigony-Neto J (2019) Open-source automatic weather station and electronic ablation station for measuring the impacts of climate change on glaciers. *HardwareX* **5**, e00053. doi: 10.1016/j.ohx.2019.e00053

Obleitner F (2000) The energy budget of snow and ice at Breidamerkurjökull, Vatnajökull, Iceland. *Boundary-Layer Meteorology* **97**(3), 385–410. doi: 10.1023/A:1002734303353

Oerlemans J (2000) Analysis of a 3 year meteorological record from the ablation zone of Morteratschgletscher, Switzerland: energy and mass balance. *Journal of Glaciology* **46**(155), 571–579. doi: 10.3189/172756500781832657

Oerlemans J, Boot W, van den Broeke MR, Reijmer CH and van de Wal RSW (2004) AWS in the ablation zones of glaciers. In *Automated Weather Stations on Glaciers*, Institute for Marine and Atmospheric Research Utrecht, Pontresina, Switzerland, 83–87.

Ohmura A (2001) Physical basis for the temperature-based melt-index method. *Journal of Applied Meteorology* **40**(4), 753–761. doi: 10.1175/1520-0450(2001)040<0753:PBFTTB>2.0.CO;2).

Paul JD, Buytaert W and Sah N (2020) A technical evaluation of LiDAR-based measurement of river water levels. *Water Resources Research* **56**(4), e2019WR026810. doi: 10.1029/2019WR026810

Pellicciotti F and 5 others (2005) An enhanced temperature-index glacier melt model including the shortwave radiation balance: development and testing for Haut Glacier d'Arolla, Switzerland. *Journal of Glaciology* **51**(175), 573–587. doi: 10.3189/172756505781829124

Popovnin VV, Danilova TA and Petrakov DA (1999) A pioneer mass balance estimate for a Patagonian glacier: Glaciar De los Tres, Argentina. *Global and Planetary Change* **22**(1), 255–267. doi: 10.1016/S0921-8181(99)00042-9

Romero M and 8 others (2022) Investigating glacier mass loss in the South Shetland Islands using open-source data loggers and off-the-shelf sensors. In *American Geophysical Union Fall Meeting*, San Francisco, CA, USA.

Saberi L and 8 others (2019) Multi-scale temporal variability in meltwater contributions in a tropical glacierized watershed. *Hydrology and Earth System Sciences* **23**(1), 405–425. doi: 10.5194/hess-23-405-2019

Schulz B (2019) Project-Symbiont-LiDAR v0.0.0. doi: 10.5281/zenodo.3766448

Schulz B (2021) *Development of an Ecosystem of Open Source Environmental Data Loggers*. Master's thesis, University of Minnesota, Minneapolis, USA.

Schulz B (2022) MCP3421 v1.0.1. doi: 10.5281/zenodo.6338647

Schulz B and Wickert AD (2020) MaxBotix_library v1.0.0. doi: 10.5281/zenodo.6338416

Schulz B and Wickert AD (2021a) Margay_library v1.0.0. doi: 10.5281/zenodo.2525457

Schulz B and Wickert AD (2021b) Project Margay v2.2.2. doi: 10.5281/zenodo.4572338

Schulz B and Wickert AD (2022a) DS3231_logger v1.0.0. doi: 10.5281/zenodo.6338628

Schulz B and Wickert AD (2022b) Project Margay: an open-source data logger for remote field deployments. *Geophysical Research Letters* **321**, 108973.

Schulz B and Wickert AD (2022c) T9602_library. doi: 10.5281/zenodo.6338379

Singh P and Kumar N (1996) Determination of snowmelt factor in the Himalayan region. *Hydrological Sciences Journal* **41**(3), 301–310. doi: 10.1080/02626669609491504

Sold L and 6 others (2021) Automated real-time ice ablation readings using in situ cameras and computer vision techniques. In *vEGU21, the 23rd EGU General Assembly*, EGU21–7663, European Geosciences Union, Vienna, Austria, doi: 10.5194/egusphere-egu21-7663

Somers LD and 8 others (2019) Groundwater buffers decreasing glacier melt in an Andean watershed—but not forever. *Geophysical Research Letters* **46**(22), 13016–13026. doi: 10.1029/2019GL084730

Stuefer M, Rott H and Skvarca P (2007) Glaciar Perito Moreno, Patagonia: climate sensitivities and glacier characteristics preceding the 2003/04 and 2005/06 damming events. *Journal of Glaciology* **53**(180), 3–16. doi: 10.3189/172756507781833848

Takeuchi Y, Naruse R and Satow K (1995) Characteristics of heat balance and ablation on Moreno and Tyndall glaciers, Patagonia, in the summer 1993/94. *Bulletin of Glacier Research* **13**, 45–56.

Tauro F and 29 others (2018) Measurements and observations in the XXI century (MOXXI): innovation and multi-disciplinarity to sense the hydrological cycle. *Hydrological Sciences Journal* **63**(2), 169–196. doi: 10.1080/02626667.2017.1420191

Temme AJ (2015) Using climber's guidebooks to assess rock fall patterns over large spatial and decadal temporal scales: an example from the Swiss Alps. *Geografiska Annaler: Series A, Physical Geography* **97**(4), 793–807. doi: 10.1111/geoa.12116

Van Wyk de Vries M, Wickert AD, Macgregor KR, Rada C and Willis MJ (2022) Atypical landslide induces speedup, advance, and long-term slowdown of a tidewater glacier. *Geology* **50**(7), 806–811. doi: 10.1130/G49854.1

Veh G and 5 others (2022) Trends, breaks, and biases in the frequency of reported glacier lake outburst floods. *Earth's Future* **10**(3), e2021EF002426. doi: 10.1029/2021EF002426

Voordendag AB and 5 others (2021) Automated and Permanent Long-Range Terrestrial Laser Scanning in a High Mountain Environment: Setup and First Results. *ISPRS Annals of the Photogrammetry, Remote Sensing and Spatial Information Sciences*, V-2-2021, 153–160. doi: 10.5194/isprs-annals-V-2-2021-153-2021

Walter MT and 5 others (2005) Process-based snowmelt modeling: does it require more input data than temperature-index modeling?. *Journal of Hydrology* **300**(1-4), 65–75. doi: 10.1016/j.jhydrol.2004.05.002

Wetterauer K, Scherler D, Anderson LS and Wittmann H (2022) Temporal evolution of headwall erosion rates derived from cosmogenic nuclide concentrations in the medial moraines of Glacier d'Otemma, Switzerland. *Earth Surface Processes and Landforms* **47**(10), 2437–2454. doi: 10.1002/esp.5386

Wheler B and 5 others (2014) Effects of temperature forcing provenance and extrapolation on the performance of an empirical glacier-melt model. *Arctic, Antarctic, and Alpine Research* **46**(2), 379–393. doi: 10.1657/1938-4246-46.2.379

Wickert AD (2014) The alog: inexpensive, open-source, automated data collection in the field. *Bulletin of the Ecological Society of America* **95**(2), 68–78. doi: 10.1890/0012-9623-95.2.68

Wickert AD (2019) MaxBotix-Helper v1.0.0. doi: 10.5281/zenodo.2653146

Wickert AD and 7 others (2022) Perito Moreno weather stations. doi: 10.5281/zenodo.7193186

Wickert AD (2023) How to build an automated ablation stake: Version 0.0.0. doi: 10.5281/ZENODO.8138911

Wickert AD and 26 others (2023) Automated Ablation Stake Data; Code and Associated Weather-station Data Included. doi: 10.5281/zenodo.7615567

Wickert AD, Sandell CT, Schulz B and Ng GHC (2019) Open-source Arduino-compatible data loggers designed for field research. *Hydrology and Earth System Sciences* **23**(4), 2065–2076. doi: 10.5194/hess-23-2065-2019

Zemp M, Hoelzle M and Haeberli W (2009) Six decades of glacier mass-balance observations: a review of the worldwide monitoring network. *Annals of Glaciology* **50**(50), 101–111. doi: 10.3189/172756409787769591